# **Article**



# Mechanical memory stored through epigenetic remodeling reduces cell therapeutic potential

Adrienne K. Scott,<sup>1</sup> Eduard Casas,<sup>2</sup> Stephanie E. Schneider,<sup>1</sup> Alison R. Swearingen,<sup>2</sup> Courtney L. Van Den Elzen,<sup>3</sup> Benjamin Seelbinder,<sup>1</sup> Jeanne E. Barthold,<sup>1</sup> Jennifer F. Kugel,<sup>4</sup> Josh Lewis Stern,<sup>4,5</sup> Kyla J. Foster,<sup>4</sup> Nancy C. Emery,<sup>3</sup> Justin Brumbaugh,<sup>2</sup> and Corey P. Neu<sup>1,6,7,\*</sup>

<sup>1</sup>Paul M. Rady Department of Mechanical Engineering, University of Colorado Boulder, Boulder, Colorado; <sup>2</sup>Department of Molecular, Cellular & Developmental Biology, University of Colorado Boulder, Boulder, Colorado; <sup>3</sup>Department of Ecology and Evolutionary Biology, University of Colorado Boulder, Boulder, Colorado; <sup>4</sup>Department of Biochemistry, University of Colorado Boulder, Boulder, Colorado; <sup>5</sup>Biochemistry and Molecular Genetics, O'Neal Comprehensive Cancer Center, University of Alabama at Birmingham, Birmingham, Alabama; <sup>6</sup>Biomedical Engineering Program, University of Colorado Boulder, Boulder, Colorado; and <sup>7</sup>BioFrontiers Institute, University of Colorado Boulder, Boulder, Colorado

ABSTRACT Understanding how cells remember previous mechanical environments to influence their fate, or mechanical memory, informs the design of biomaterials and therapies in medicine. Current regeneration therapies, such as cartilage regeneration procedures, require 2D cell expansion processes to achieve large cell populations critical for the repair of damaged tissues. However, the limit of mechanical priming for cartilage regeneration procedures before inducing long-term mechanical memory following expansion processes is unknown, and mechanisms defining how physical environments influence the therapeutic potential of cells remain poorly understood. Here, we identify a threshold to mechanical priming separating reversible and irreversible effects of mechanical memory. After 16 population doublings in 2D culture, expression levels of tissue-identifying genes in primary cartilage cells (chondrocytes) are not recovered when transferred to 3D hydrogels, while expression levels of these genes were recovered for cells only expanded for eight population doublings. Additionally, we show that the loss and recovery of the chondrocyte phenotype correlates with a change in chromatin architecture, as shown by structural remodeling of the trimethylation of H3K9. Efforts to disrupt the chromatin architecture by suppressing or increasing levels of H3K9me3 reveal that only with increased levels of H3K9me3 did the chromatin architecture of the native chondrocyte phenotype partially return, along with increased levels of chondrogenic gene expression. These results further support the connection between the chondrocyte phenotype and chromatin architecture, and also reveal the therapeutic potential of inhibitors of epigenetic modifiers as disruptors of mechanical memory when large numbers of phenotypically suitable cells are required for regeneration procedures.

SIGNIFICANCE Tissue regeneration procedures, such as cartilage defect repair (e.g., matrix-induced autologous chondrocyte implantation), often require cell expansion processes to achieve sufficient cells to transplant into an in vivo environment. However, the chondrocyte cell expansion on 2D stiff substrates induces epigenetic changes that persist even when the chondrocytes are transferred to a different (e.g., 3D) or in vivo environment. Treatments to alter epigenetic gene regulation may be a viable strategy to improve existing cartilage defect repair procedures and other tissue engineering procedures that involve cell expansion.

#### INTRODUCTION

Cells constantly sense and adapt to cues from the mechanical environment, affecting cell function, differentiation, and disease states. Many studies have explored how the physical and mechanical properties of the environment affect cellular

 $Submitted \, September \, 20, \, 2022, \, and \, accepted \, for \, publication \, March \, 1, \, 2023.$ 

\*Correspondence: cpneu@colorado.edu

Editor: Guy Genin.

https://doi.org/10.1016/j.bpj.2023.03.004

© 2023 Biophysical Society.

behavior (1,2); however, little is known about how cellular adaptations from previous physical environments are maintained or how cells encode mechanical memory. The key to mechanical memory is to understand how physical priming in one environment will impact cellular performance and fate in another, later environment (3–5). In some cases, when exposure to physical priming is limited, mechanical memory can persist for a short time period (e.g., 1–3 days) and does not impact long-term cell fate (6). In contrast, when the exposure time to a mechanical



environment increases past a critical threshold, the accumulated memory of this environment reduces cellular plasticity, resulting in cells reprogrammed to a state with a persisting phenotype (4,7,8). In some cases, this reprogrammed state can be maladaptive and can aggravate diseases such as fibrosis (4,7,9), influence cellular behavior of cancer metastasis (10), or limit tissue regeneration procedures (4-6). However, mechanisms of mechanical memory are not well understood, and investigating how to disrupt maladaptive mechanical memory for translational applications is critical.

Our studies focus on the impact of mechanical memory on tissue regeneration therapies, such as cartilage defect repair procedures. Various standard tissue engineering procedures involve culturing cells on 2D tissue culture plastic (TCP) to generate sufficient cells to transplant into an in vivo environment. However, this expansion and associated mechanical priming alters cell fate in vivo (4,11), suggesting that there is an exposure limit to in vitro culture expansion before the memory of this environment alters the cells' therapeutic potential. Monolayer expansion in vitro is a crucial step in some cartilage defect repair procedures, such as MACI (matrix-induced autologous chondrocyte implantation) (12,13). This procedure is considered safe and effective, but the repair often results in the formation of fibrocartilage, which is mechanically inferior to hyaline (native) cartilage. MACI involves three steps: 1) isolating a biopsy taken from a nonload-bearing region of the knee, 2) expanding chondrocytes on TCP up to 16 population doublings to acquire 0.5–1 million cells per cm<sup>2</sup> of defect region (14), and 3) seeding cells onto a porcine collagen matrix for implantation into the defect (15). While native chondrocytes are mostly quiescent cells, the exposure to a stiff 2D substrate in vitro causes chondrocytes to proliferate. Although the proliferation is beneficial to generate sufficient cells for the MACI procedure, the exposure to stiff 2D substrates is known to cause chondrocytes to dedifferentiate, meaning that the hyaline chondrocyte phenotype is lost and a fibroblast-like phenotype emerges (12,16,17). Previous work from our lab suggests that 2D culture influences the chondrocyte phenotype through changes in nuclear strain transfer (18). In fact, when the 3D geometry and physiological nuclear strains are restored following transfer to a 3D scaffold after dedifferentiation, it is well known that the round chondrocyte hyaline morphology returns (19). However, it is unknown how long the expansion process influences cell fate of the chondrocytes when transferred to a 3D scaffold and if the chondrogenic phenotype can be fully restored (12,20). In this article, we define the ability to regain the primary chondrocyte phenotype, through gene expression of chondrogenic genes, as a measure of chondrogenic potential (21). Previous studies have not yet explored how stiff mechanical priming may instill mechanical memory leading to a fibrotic repair and preventing proper regeneration of cartilage, motivating us to understand the extent to which chondrocytes demonstrate mechanical memory and how to prevent this maladaptation to restore the therapeutic potential of expanded chondrocytes.

Though mechanisms of mechanical memory are poorly understood, recent studies focus on the organization of chromatin architecture within the nucleus (3,5,8,22). Therefore, changes in spatial organization of chromatin or chromatin architecture could retain the persisting memory of the dedifferentiated chondrocyte state. Chromatin architecture is mediated by various epigenetic factors, such as DNA methylation or posttranslational modifications of histones. Our studies explore the chromatin architecture of repressive histone modification, H3K9me3, a heritable epigenetic marker that mediates cellular memory and cell fate in many cell types (23–26). H3K9me3 both restricts cellular reprogramming (27) and is remodeled in chondrocytes (28) and other cell types (29) in response to a change in the biophysical environment. We hypothesized that expanding chondrocytes in vitro would result in the remodeling of H3K9me3-marked chromatin that persists even in different physical environments, establishing a mechanical memory in chondrocyte cells.

The objective of this study is to investigate the extent to which chromatin remodeling, through spatial analysis of H3K9me3 occupation in the nucleus, is associated with the chondrocyte phenotype and retains a memory from the in vitro expansion process on 2D stiff substrates. This memory may limit the therapeutic potential of chondrocytes, specifically in the context of cartilage defect repair procedures. Throughout the in vitro culture on TCP, we show that the chromatin architecture of regions enriched with histone modification H3K9me3 progressively change while the chondrocyte phenotype is lost. When dedifferentiated chondrocytes are encapsulated in a 3D environment, the gene expression profile and chromatin architecture is retained in a dose-dependent manner, suggesting a structural epigenetic memory from the previous environment. Using an inducible mouse model to suppress levels of H3K9me3, we find that decreasing the levels of H3K9me3 does not stop the dedifferentiation process, but it also does not prevent nuclear structural changes. However, by increasing the levels of H3K9me3 through inhibition of the demethylases of H3K9 (KDM4 enzymes), chondrocyte dedifferentiation is attenuated, and main features of the hyaline chondrocyte chromatin structure are retained.

# **MATERIALS AND METHODS**

# 2D cell culture of bovine chondrocytes

We harvested chondrocytes from cartilage extracted from juvenile bovine stifle (2-week-old knee) joints within 12 h of slaughter. Using aseptic techniques (30,31), we harvested the cartilage of the femoral medial condyles, ensuring that the cells from each animal were kept separate. We rinsed obtained tissue three times with sterile PBS (Hyclone, Logan, UT, USA, cat. no. SH30028.03) and digested the tissue with 0.2% collagenase-P (Roche Pharmaceuticals, Basel, Switzerland, 11213873001) for 5-6 h at 37°C with agitation (230 Rpm). After the digestion, we quenched the digested tissue with media and filtered with a 70 µm filter (Fisher, cat. no. 22363548, Thermo Fisher Scientific, Waltham, MA) to remove extracellular material and isolate chondrocytes. Chondrocyte media consisted of chemically defined DMEM/F12 (Gibco, cat. no. 11330-032) supplemented with 10% fetal bovine serum (Gibco, cat. no. 26140-079), 0.1% bovine serum albumin (Sigma, Burlington, MA, USA, cat. no. A9418-100g), 1× penicillin/streptomycin (Gibco, cat. no. 15140-122) and 50 μg/mL ascorbate-2-phosphate (Sigma, cat. no. 49752-10G) (31). We seeded chondrocytes on TCP (Corning, Corning, NY, USA, cat. no. 430167, or Ibidi, Fitchburg, WI, USA, cat. no. 8084) at a density of  $4 \times 10^4$  cells/cm<sup>2</sup> and expanded the cells for up to 16 population doublings (PD16). Cells were passaged around 80% confluency. All samples were incubated at 37°C and 5% CO2 in chondrocyte media.

# 3D cell culture of bovine chondrocytes

We encapsulated chondrocyte cells after isolation (PD0), passage 2 (PD8), and passage 4 (PD16) in 3D hyaluronan-poly(ethylene) glycol diacrylate (HA-PEGDA) hydrogels and cultured for 1, 5, and 10 days. Chondrocytes were culture for 10 days in 3D culture since previous studies exploring mechanical memory observed persisting or reversible phenotypes by 10 days (5,6). To make HA-PEGDA hydrogels, we lyophilized 23%-25% thiolated HA (Lifecore Biomedical, Chaska, MN, USA, cat. no. HA100k-5), dissolved the HA in sterile PBS, and combined the HA with a PEGDA (Alfa Aesar, Stoughton, MA, USA, cat. no. 46497, molecular weight = 3400 Da) solution (32). We used a final concentration of 20 mg/1 mL HA and 8.6 mg/mL PEGDA, resulting in a ratio of 1:0.8 thiol groups to PEGDA. In the HA-PEGDA gel, we encapsulated cells at a concentration  $20 \times 10^6$  cells/mL in 100 μl gels. Next, we cultured the encapsulated cells at 37°C for 30 min to facilitate the cross-linking between the diacrylate groups on the PEGDA molecule and the thiol groups on the thiolated HA molecule, and then further maintained them at 37°C and 5% CO<sub>2</sub> in chondrocyte media. To name each sample, we abbreviated encapsulated cells by the number of PDs undergone before encapsulation and denoted these samples with "3D" because they were cultured in a 3D culture. For example, cells encapsulated in HA-PEGDA hydrogels after PD8 on TCP are abbreviated as PD8-3D cells.

# 2D cell culture of H3K9M and H3WT murine chondrocytes

For H3.3 lysine-to-methionine mutant (H3K9M) and wild-type H3.3 (H3WT; control) studies, male mice carrying the transgene (33) were bred to C57BL/6 (Jackson Laboratory, Bar Harbor, ME, USA, cat. no. 000664) female mice. The methods were performed in accordance with relevant guidelines and regulations and approved by the Institutional Animal Care and Use Committee. Mice were maintained in specific-pathogen-free, temperature-controlled housing with 12 h light cycles and received food and water ad libitum. Chondrocytes from embryonic (embryonic day 18.15) H3K9M and H3WT mice were harvested and cultured with chondrocyte media and 2 µg/mL doxycycline (Sigma, cat. no. D3072-1mL) for PD0, PD8, and PD16 on TCP (Corning, cat. no. 430165, or Ibidi, cat. no. 80841). To harvest embryonic chondrocytes, hind limb articular cartilage was isolated and washed 3× with PBS, transferred to 3 mg/mL collagenase-P solution in DMEM F12 (with 1× penicillin/streptomycin), digested for 12 hr at 37°C, filtered through a 70 µm mesh strainer, and plated at a density of  $4 \times 10^4$  cells/cm<sup>2</sup> (34).

# Immunofluorescence staining and imaging

We fixed cells cultured on TCP in 4% paraformaldehyde (PFA; Electron Microscopy Sciences, Hatfield, PA, USA, cat. no. 15714-S) for 10 min and permeabilized them in 1% Triton-X100 (Sigma, cat. no. 78787-100mL) in PBS for 10 min (29). Before incubating with the primary antibodies, we blocked by incubating the cells with 10% natural goat serum (Invitrogen, Waltham, MA, USA, cat. no. 10000C), 1% bovine serum albumin (BSA) in 0.1% PBT (0.1% Tween-20, Bio-Rad, Hercules, CA, USA, cat. no. 170-6531, in PBS) for 60 min at room temperature (RT). We performed the primary antibody incubation in 0.1% PBT containing 1% BSA at 4°C overnight (12 h) and the H3K9me3 primary antibody (Abcam, Camrbdige, UK, ab8898, 1:600) with agitation. Following the primary incubation, we performed the secondary incubation in 0.1% PBT containing 1% BSA, with Alexa Fluor 633 goat anti-rabbit immunoglobulin G (Life Technologies, Carlsbad, CA, USA, cat. No. A21070) at a dilution of 1:500 for 45 min (RT) with agitation. To visualize both actin and DNA, we counterstained with 488 Phalloidin (Invitrogen, cat. no. A12379, 1:80, 20 min incubation in PBS) and DAPI (Invitrogen, cat. no. D1306, 1:1000, 10 min incubation in PBS), respectively.

To stain cells encapsulated in 3D HA-PEGDA hydrogels, we used a similar protocol. However, we fixed the cells in 4% PFA for 30 min, permeabilized them in 1% Triton-X100 in PBS for 15 min, and blocked them with 5% natural goat serum and 1% BSA in 0.1% PBT for 60 min. The primary antibody incubation was performed in 0.1% PBT containing 1% BSA at 4°C for 16 h with agitation. We used the same primary and secondary antibodies listed previously. Secondary incubation was also performed in 0.1% PBT containing 1% BSA at a dilution of 1:200 for 2 h (RT) with agitation. Lastly, we counterstained both actin and DNA with 488 Phalloidin (1:80, 40 min incubation in PBS) and DAPI (1:500, 15 min incubation in PBS), respectively.

Using an inverted Nikon A1R confocal microscope with a 60× oil immersion objective, we imaged both encapsulated cells and cells grown on TCP from all time points, treatments, and genotypes (Figs. 1 and 2). Specifically, we imaged the nucleus/DNA (DAPI; 405 nm), actin (phalloidin; 488 nm), and H3K9me3 (640 nm).

#### Image-based structural nuclear analysis

Using a custom MATLAB (R2020a) code, we analyzed imaged nuclei from each experimental group (n < 15 nuclei/experimental group/animal). For each nucleus, the nucleus was segmented using a reference (DAPI, 405 channel) signal, and intensity values were normalized according to previously established methods (29). The nuclear area and aspect ratio were calculated using the MATLAB image processing toolbox. H3K9me3 foci were detected by finding the local maxima in each segmented nucleus in the H3K9me3 signal (640 channel) using the MATLAB script FastPeakFind (v.1.13.0.0) (35). Detected peaks were counted as H3K9me3 foci. To track the change in location of the foci for the cell treated with ML324 or DMSO, the distance to the center of the nucleus (a) and the distance from the nuclear periphery (b)were calculated for each detected H3K9me3 foci. The ratio of a/(a+b) was calculated to determine the relative location of each foci relative to the center of the nucleus. MATLAB code is available upon request from the corresponding author.

# Gene expression assessed with quantitative realtime PCR

We quantified expression of previously established genes that change during chondrocyte dedifferentiation (COL2A1, COL1A1, ACAN, SOX9, VCAN, THYI). Total RNA was isolated from both 3D and 2D cultures to assess relative gene expression using quantitative real-time PCR. To isolate RNA from 3D cultures, we homogenized the HA-PEGDA matrices using a Tissue Ruptor for 30 s in QIAzol lysis reagent (Qiagen, Germantown, MD, USA, cat. no. 79306) (36). Lysed cells from 2D cultures on TCP were collected in QIAzol. After lysis, we extracted the total RNA with the E.Z.N.A. Total RNA kit (Omega Tek, Norcross, GA, USA, cat. no. R6834-01) or the Direct-zol RNA MiniPrep (Zymo Research, Irvine, CA,

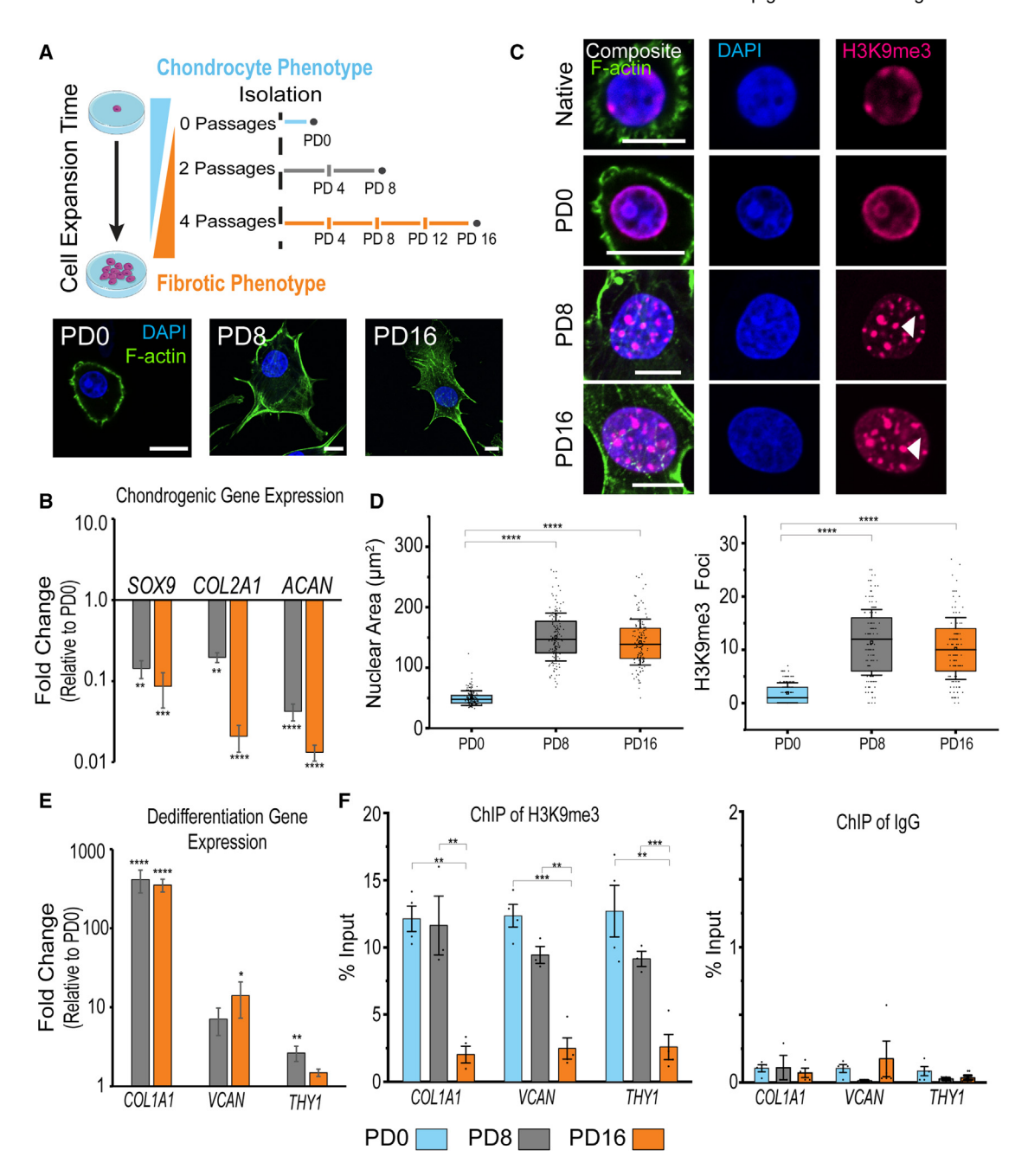


FIGURE 1 Extended culture on stiff substates leads to global remodeling of trimethylated H3K9 and a decrease in levels of H3K9me3 locally on dedifferentiation marker genes. (A) Bovine chondrocytes were isolated and plated on tissue culture plastic (0 population doublings [PD0]), passaged two times (PD8), and passaged 4 times (PD16). As PDs increased, chondrocytes dedifferentiated into fibroblast-like cells. PD8 and PD16 chondrocytes became more spread out (scale: 5  $\mu$ m). (B) Expression of hallmark chondrogenic genes (SOX9, COL2A1, and ACAN) decreased (mean  $\pm$  SE, N=6 biological replicates). (C) Chondrocytes expanded in a 2D stiff environment show changes in chromatin architecture reorganization (DAPI) and H3K9me3 location and distribution (scale: 10 µm). Chromatin architecture of PD0 cells and native chondrocytes imaged ex vivo was similar. White indicators highlight H3K9me3 foci. (D) With increased time on 2D stiff substrates, both nuclear area and the number of H3K9me3 foci increased ( $\pm$  SD, N=6 biological replicates, n>22 nuclei/treatment/replicate). (E) Expression of dedifferentiation markers (COLIA1, VCAN, and THY1 mRNA levels) increased compared with PD0 cells (mean ± SE, N = 6 biological replicates). (F) Occupancy levels of H3K9me3 on the promoters of dedifferentiation genes decreased with PDs, while the background (immunoglobulin G) remained low, potentially allowing for increased expression of these genes in the PD16 state ( $\pm$  SD, N = 3–4 biological replicates). \*p < 0.05, \*\*p < 0.01, \*\*\*p < 0.001, \*\*\*\*p < 0.0001. To see this figure in color, go online.

USA, cat. no. R2050). To reverse transcribe the isolated RNA to cDNA, we used iScript Reverse Transcription Supermix (Bio-Rad, cat. no. 1708841). Quantitative real-time PCR was performed using Sso AdvancedTM Universal SYBR Green Supermix (Bio-Rad, cat. no. 1725271) in a CFX96 Touch adthermocycler (Bio-Rad). We designed all primers (sequences listed in Table S4) using NCBI primer blast, ensuring that all primers spanned an exon-exon junction and were specific for all known splice variants and that the efficiency of all primers was calculated to be above 90%. Integrated

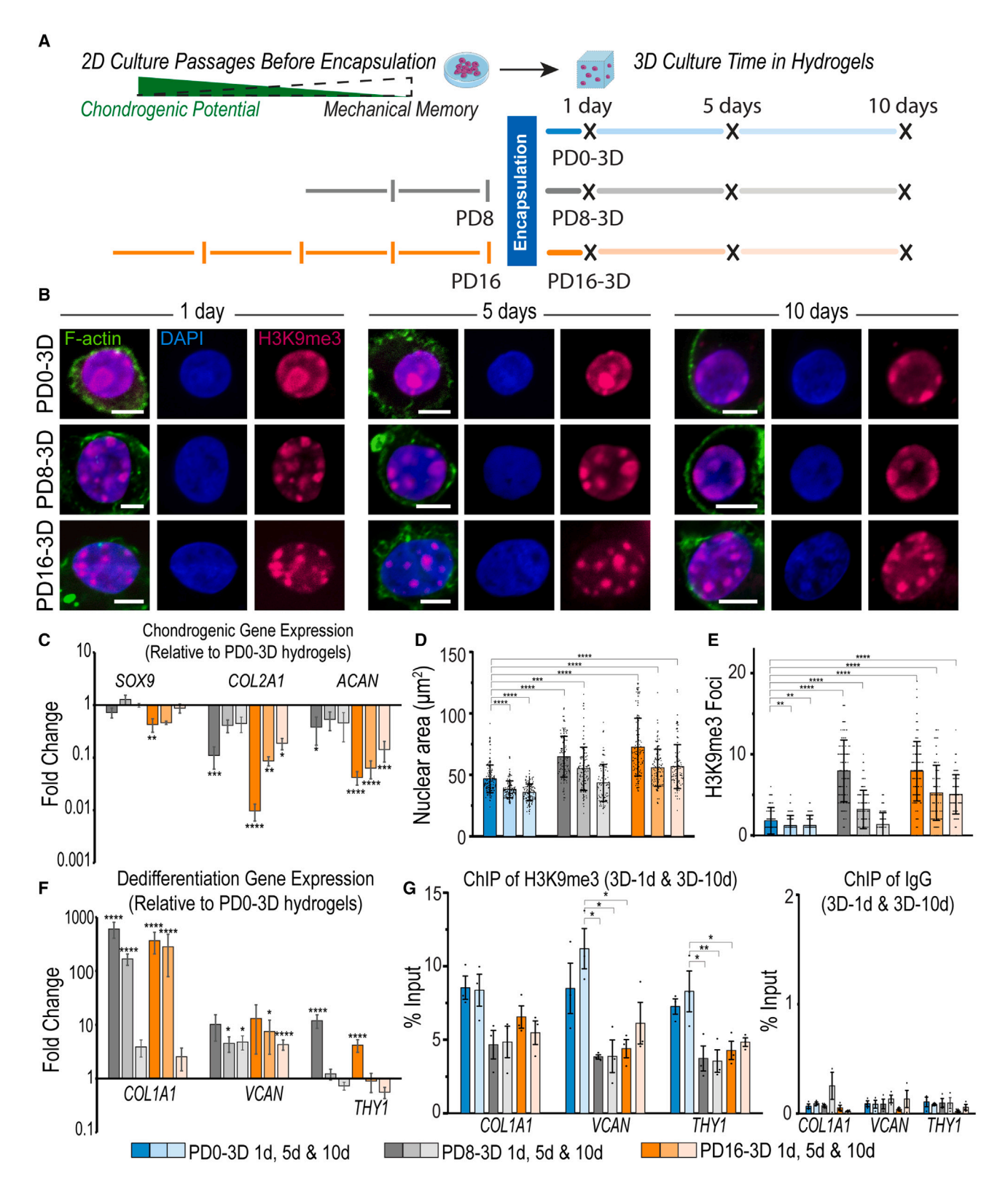


FIGURE 2 Expanded chondrocytes encapsulated in 3D hydrogels exhibited a dose-dependent mechanical memory shown by chondrogenic gene expression and H3K9me3 nuclear architecture but not local gene regulation of dedifferentiation markers. (*A*) After 0, 8, and 16 chondrocyte PDs, cells were encapsulated into hydrogels and cultured for 1, 5, and 10 days (PD0-3D, PD8-3D, PD16-3D). (*B*) Cells were stained for H3K9me3 to assess chromatin architecture adaptations in 3D culture (scale: 5  $\mu$ m). (*C*) Chondrogenic potential was assessed by changes in gene expression of chondrogenic genes of PD8-3D and PD16-3D cells compared with PD0-3D cells. Although chondrogenic gene expression (*COL2A1*, *ACAN*) of PD16-3D cells did not return to levels of PD0-3D cells after 10 days, the gene expression of PD8-3D cells did return to levels similar to PD0-3D cells after 5 or 10 days in culture, indicating a

(legend continued on next page)

DNA Technologies (Coralville, IA, USA) performed the synthesis of primers. We normalized all data to the average of reference genes, HPRT1 and GAPDH. To evaluate the relative change in gene expression, we used the  $\Delta\Delta Ct$  method.

# RNA sequencing (RNA-seq) gene expression

H3K9M and H3WT chondrocytes were cultured in the presence of doxycycline (2  $\mu$ g/mL) for PD16 and lysed with Qiazol, and RNA was extracted using Direct-zol RNA MiniPrep (Zymo Research, cat. no. R2050). Poly A-selected RNA was sequenced at the Genomics Shared Resource Facility at UC Anschutz Medical Campus (Aurora, CO, USA). We mapped reads using hisat2 v.2.1.0 (37) and custom parameters to the UCSC mouse genome release mm10. We summarized reads to genes annotated by UCSC using featureCounts v.1.6.2 (38). We further assessed count data in R 3.6 using DE-Seq2 (39) to analyze differentially expressed genes and used clusterProfiler (40) for the gene set enrichment analysis of Gene Ontology pathways. We compared our data with publicly available RNA-seq data of embryonic proliferating chondrocytes (41) using in-house scripts based on DeepTools (42) and the bamTools and bedTools suite. Our RNA-seq data are found on the NIH GEO database (GEO: GSE190339).

## Chromatin immunoprecipitation (ChIP)

For adherent chondrocyte cells cultured on 2D, we crosslinked  $2\times10^6$ - $4\times10^6$ cells in 1% PFA in PBS for 10 min, quenched in 150 mM glycine (Fisher, Cat. No. BP381-500), and scraped to harvest the cells. To harvest cells from the HA-PEGDA hydrogels, we followed a protocol for harvesting tissues for ChIP (43). Briefly, we homogenized the hydrogels using a disposable plastic pestle in ice cold PBS. Then, we crosslinked the cells with 1% methanol-free formaldehyde for 15 min with agitation and quenched in 150mM glycine. Next, we harvested the hydrogels by centrifugation at 2000g for 10mins.

We lysed both 2D and 3D cultured cells in lysis buffer, 50 mM Tris-Cl (Sigma, 93,363-50G), 10mM EDTA (Fisher, Cat. No. BP120-1), 0.5% SDS (Sigma, Cat. No. L3771-100g), 1× Protease Inhibitor (Sigma, Cat. No. SRE0055-1BO). Then, we sheared the chromatin by sonicating the samples in a Bioruptor UCD-200 (Diagenode) or an M220 Focused Ultrasonicator (Covaris) so that fragment sizes of chromatin were between 200 bp to 500 bp. After shearing, we added 20  $\mu$ g of chromatin to IP buffer (16.7 mM Tris-Cl, 1.2 mM EDTA, 167 mM NaCl (Fisher, Cat. No. S271-500), 1% Triton X-100). We performed ChIP on both cells cultured in 3D and on 2D (44) with 2  $\mu g$  of ChIP validated antibody for the protein of interest, H3K9me3 (abcam, ab8898), as well as negative control non-specific immunoglobulin G (Millipore, Cat. No. 12370) and a positive control H3 (abcam, Cat. No. ab1791) antibodies. Antibody chromatin complexes were incubated overnight with rotation. Protein A/G magnetic beads (Pierce, Cat. No. 88803) were then added for 3 h at 4°C with rotation. We washed the beads with a series of buffers: low Salt Buffer (20 mM Tris-Cl, 2mM EDTA, 150 mM NaCl, 0.1% SDS, 1% Triton X-100), High Salt Buffer (20 mM Tris-Cl, 2mM EDTA, 500 mM NaCl, 0.1% SDS, 1% Triton X-100), LiCl Buffer (10mM Tris-Cl, 1mM EDTA, 250 mM LiCl; Sigma, Cat. No. L9650-100G), 1% Sodium Deoxycholate (Sigma, Cat. No. D2510-100G), 1% IGEPAL (Sigma, Cat. No. 18896-50ML)). We eluted the chromatin in elution buffer (1% SDS, 100mM NaHCO3; Fisher Cat. No. S233-500), and added 5  $\mu$ L of 5 M NaCl to reverse the crosslinking during an overnight incubation at 65°C. Protein and RNA was digested with Proteinase K (Ambion Life Technology, Cat. No. AM2542) and RNAse A (Ambion Life Technology, Cat. No. AM2272) before the DNA was purified with either DNA clean and concentrator kit (Zymo, Cat. No. D5201) or phenol chloroform (VWR, Cat. No. 97064-692) extraction and ethanol precipitation. We analyzed the purified DNA using qPCR with primers designed to amplify the promoter regions of the following genes, COL1A1, THY1, VCAN. We designed the DNA primers (Table S5) using NCBI primer blast and ordered the primers from Integrated DNA Technologies. To determine the relative enrichment of each protein of interest for the specified promoter regions, we calculated the percent input, or the signal of an IP sample relative to the qPCR signal from the input samples (samples without IP)

#### Western blot

Following PD16, H3K9M and H3WT chondrocytes were prepared for Western blot analysis by nuclear isolation following a previously reported protocol (29). Briefly, cells were resuspended in cold nuclear isolation buffer (50 mM Tris-HCl pH 8, 15 mM NaCl, 60 mM KCl, 5 mM MgCl<sub>2</sub>, 1 mM CaCl<sub>2</sub>, 250 mM sucrose, 1 mM dithiothreitol, 0.6% IGEPAL (Sigma-Aldrich)) supplemented with complete protease inhibitors (Sigma-Aldrich) and incubated for 5 min on ice. Isolated nuclei were then centrifuged (960 × g for 5 min), washed in nuclear isolation buffer and lysed in RIPA buffer (50 mM Tris-HCL (pH 8), 150 mM NaCl, 0.1% SDS, 0.5% sodium deoxycholate, 1% Triton X-100 and 1 mM EDTA (all from Sigma-Aldrich) supplemented with complete protease inhibitors (Sigma-Aldrich) and 0.01 U µl-1 benzonase (Novagen). We sonicated the resulting lysates 10 times for 30 s with a 30 s pause between pulses using a Bioruptor Pico sonicator (Diagenode). The lysates were then cleared to remove cell debris through centrifuging and collecting the supernatant which was boiled together with Laemmli sample buffer (100 mg mL-1 SDS, 250 mM Tris pH 6.8, 1 mg mL-1 bromophenol blue and 50% glycerol (all from Sigma-Aldrich) and loaded into 4-20% mini-Protean TGX precast protein gels (BioRad). Protein was transferred to PVDF membranes (Bio-Rad) and blocked for 1 h in 5% powdered milk in Tris-buffered saline and Tween-20. The following primary antibodies were used: H3K9me3 (Abcam, 8898; 1:1000), H3 (Abcam, 1791; 1:10,000 dilution). Goat, anti-rabbit-HRP-conjugated (Invitrogen, PI31460; 1:2000 dilution) was used as the secondary antibody. Immobilon western chemiluminescent HRP substrates (Millipore) were used to detect proteins.

# ML324 treatment

Twenty-four hours after seeding isolated chondrocytes (PD0), we treated the cells with chondrocyte medium supplemented with 10  $\mu$ M of ML324 (45) (MedChemExpress, Cat. No. HY-12725) or a carrier control DMSO (Sigma, Cat. No. 276855-100mL) and continued to supplement the media throughout the expansion process. All inhibitors were dissolved in DMSO (final concentration <0.1%, which has been shown to not change basic metabolic activity and cell proliferation) (46), and we confirmed that the DMSO did not significantly affect cell viability (Fig. S3 B). Control culture medium contained 0.1% DMSO. We collected cells for imaging and gene expression analysis on PD0 (24hrs after isolation), PD8 and PD16.

dose-dependent genetic memory from the previous culture (mean  $\pm$  SE, N=6 biological replicates). (D) Quantified nuclear area ( $\pm$  SD, N=6 biological replicates, n > 16 nuclei/treatment/replicate, only p values for P0-1D comparisons are shown for clarity, Table S1 reports all p values) and (E) number of H3K9me3 foci was restored to levels of the P0-3D cells only with lower PDs (PD8-3D cells only), demonstrating a mechanical memory from the expansion process on a stiff 2D substrate ( $\pm$  SD, N=6 biological replicates, n>16 nuclei/treatment/replicate, only p values for P0-1D comparisons are shown for clarity, Table S1 reports all p values). (F) Expression of dedifferentiation genes decreased to levels of PD0-3D cells for both PD8-3D and PD16-3D cells; however, the expression of these genes did not show a dose-dependent memory (mean  $\pm$  SE, N=6 biological replicates). (G) ChIP results of PD8-3D and PD16-3D cells revealed a persistent lower occupancy level of H3K9me3 (with low immunoglobulin G background) on the promoters of the dedifferentiation genes compared with PD0-3D cells, which did not change after 10 days ( $\pm$  SD, N=3 biological replicates). \*p < 0.05, \*\*p < 0.01, \*\*\*p < 0.001, \*\*\*\*p < 0.0001. To see this figure in color, go online.

## Statistical analysis

All statistical testing was performed using R (version 4.0.3) and Rstudio (version 1.3.1093) software. All datasets (number of foci, nuclear area, nuclear aspect ratio, ChIP results, gene expression results, foci location) were analyzed using a linear mixed effect model (nlme package, version 3.1-149) with a type II or III sum of squares ANOVA using the containment method for estimating denominator degrees of freedom (car package, version 3.0-10). Type III ANOVA was used when the model contained an interaction term (Fig. 4 C, D, E, and F) and a type II ANOVA was used for all other linear models. Each model contained Doubling Time and/or Treatment as fixed effects and we allowed the model intercept to vary with the experimental animal to control for difference among animals. Normality of the residuals was evaluated using the Shapiro-Wilk test and, if necessary, the response was transformed to meet the assumptions of the model. Specifically, nuclear area measurements (Figs. 1 D, 2D, 3C,4C and S4B) were transformed using a square root function (measurement (1/2), nuclear aspect ratio measurements (Figs. S1, 4 B) were transformed using a natural log function (ln(measurement)) and the foci location data was transformed using a arcsine-square root transformation (arcsin(mea $surement^{(1/2)}$ )). All Shapiro-Wilk test statistics (W) values for the final models were greater than 0.9, meeting the assumption of normality of residuals. Additionally, homogeneity of the residual variance was evaluated for each data set by plotting the residuals against the fitted values of the linear model. In some models (number of foci: Figs. 1 D, 2 E, 3 C, and 4 D, nuclear area: Figs. 1 D, 2 D, 3 C, 4 C and S4 B, nuclear aspect ratio: Figs. S1, 4 B) the variance was dependent on the PD level, so a heterogeneous variances model was used to allow for differences in variance among the groups. The use of the heterogeneous variance model was also justified when the likelihood ratio test showed a significant difference (p > 0.05) between the heterogeneous variance model and the linear mixed model with constant variance. We then used the emmeans function (package emmeans, version 1.5.3) to calculate the estimated marginal means and test whether each treatment levels was statistically significantly different from each other level, accounting for the differences in variance. The containment method was again used for estimating denominator degrees of freedom. p values were adjusted for multiple comparisons using the Tukey method. A p-value less than 0.05 was considered significant, and significance was denoted as \*p < 0.05, \*\*p < 0.01, and \*\*\*p < 0.001, \*\*\*\*p < 0.0001. Note the linear model of data with low numbers of samples may have too low of power to determine accurate p-values when the effect size is small (Fig. 1 F, comparison between PD0 and PD8). However, when the effect size is large enough (Fig. 1 F, comparison between PD0 and PD16), the p-values are considered accurate.

# RESULTS

# H3K9me3 marked chromatin spatially remodeled on 2D stiff substrates during expansion

To understand how the nucleus changed in response to the mechanical environment, we first analyzed the bulk nuclear morphology and intranuclear organization of bovine chondrocytes during expansion on a stiff 2D substrate (TCP). We confirmed the dedifferentiated phenotype reported in literature (12,47) by observing the cellular morphology (cell spreading and actin reorganization) and assessing the change in mRNA expression of hallmark chondrogenic genes (ACAN, SOX9, COL2A1) compared to chondrocytes analyzed after isolation (Fig. 1 A, and B). As the chondrocytes dedifferentiated, we observed that the nuclear area and nuclear aspect ratio increased (Figs. 1 C, D S1 A). By staining DNA using DAPI, we found that the chromatin architecture spatially differed between chondrocytes after isolation (PD0) and after PD16 (Fig. 1 C, middle column). Specifically, euchromatin regions (low intensity DAPI signal) were located in the center of the nucleus, while heterochromatin regions (high intensity DAPI signal) were located toward the nuclear envelope. The structural reorganization of heterochromatin and euchromatin suggested that expansion time on TCP influenced mechanisms associated with regulating chromatin architecture and gene expression (e.g. histone modifications, DNA methylation).

Because we observed a change in heterochromatin organization, we next studied the specific arrangement of H3K9me3, a marker of heterochromatin, during chondrocyte dedifferentiation. We were also motivated to study H3K9me3 specifically because this repressive histone modification is crucial for the regulation of cell fate (23–26) and has been shown to remodel in response to changes in the mechanical environment (28). We hypothesized that expanding chondrocytes in vitro would result in remodeling of H3K9me3 marked chromatin and this change in chromatin architecture would influence cell fate. We first observed that H3K9me3 was localized near the nuclear envelope of the PD0 chondrocyte, but during dedifferentiation the regions of H3K9me3 formed more distinct foci distributed evenly throughout the nucleus (Fig. 1 C). We confirmed that the PD0 chromatin architecture state resembled the native chondrocyte by imaging chondrocytes in native tissue and also found low levels of H3K9me3 foci and an occupation of H3K9me3 toward the nuclear envelop (Figs. 1 C, S4 A, and B). Although the occupation of H3K9me3 toward the nuclear envelop was not as prominent in the chondrocyte images in vivo (Figs. 1 C, S4 A, and B), this observation may be partially due to the limitations of imaging through dense cartilage tissue. To quantify the overall structural shift from the native chondrocyte chromatin architecture to the dedifferentiated chromatin architecture state, we used a custom MATLAB code to analyze the number of H3K9me3 foci in the imaged nuclei (Fig. 1 D) and found the average number of H3K9me3 foci in each nucleus increased with exposure time to the 2D stiff environment.

# Occupation levels of H3K9m3 decreased on chondrocyte dedifferentiation genes by PD16

Because of the observed spatial reorganization of H3K9me3 during passaging, we explored whether this epigenetic modification mediates typical chondrocyte specific changes in gene expression during the dedifferentiation process. Using chromatin immunoprecipitation (ChIP) in conjunction with qPCR, we found that occupancy levels of H3K9me3 on promoters of chondrogenic genes (SOX9, COL2A1, ACAN) of PD0 cells were close to background levels, which was expected since these genes were highly expressed at PD0 (Fig. S2 A). By PD16, the levels of H3K9me3 occupancy did not increase on the promoters of SOX9, COL2A1, or ACAN, indicating that H3K9me3 did not suppress these chondrogenic genes during

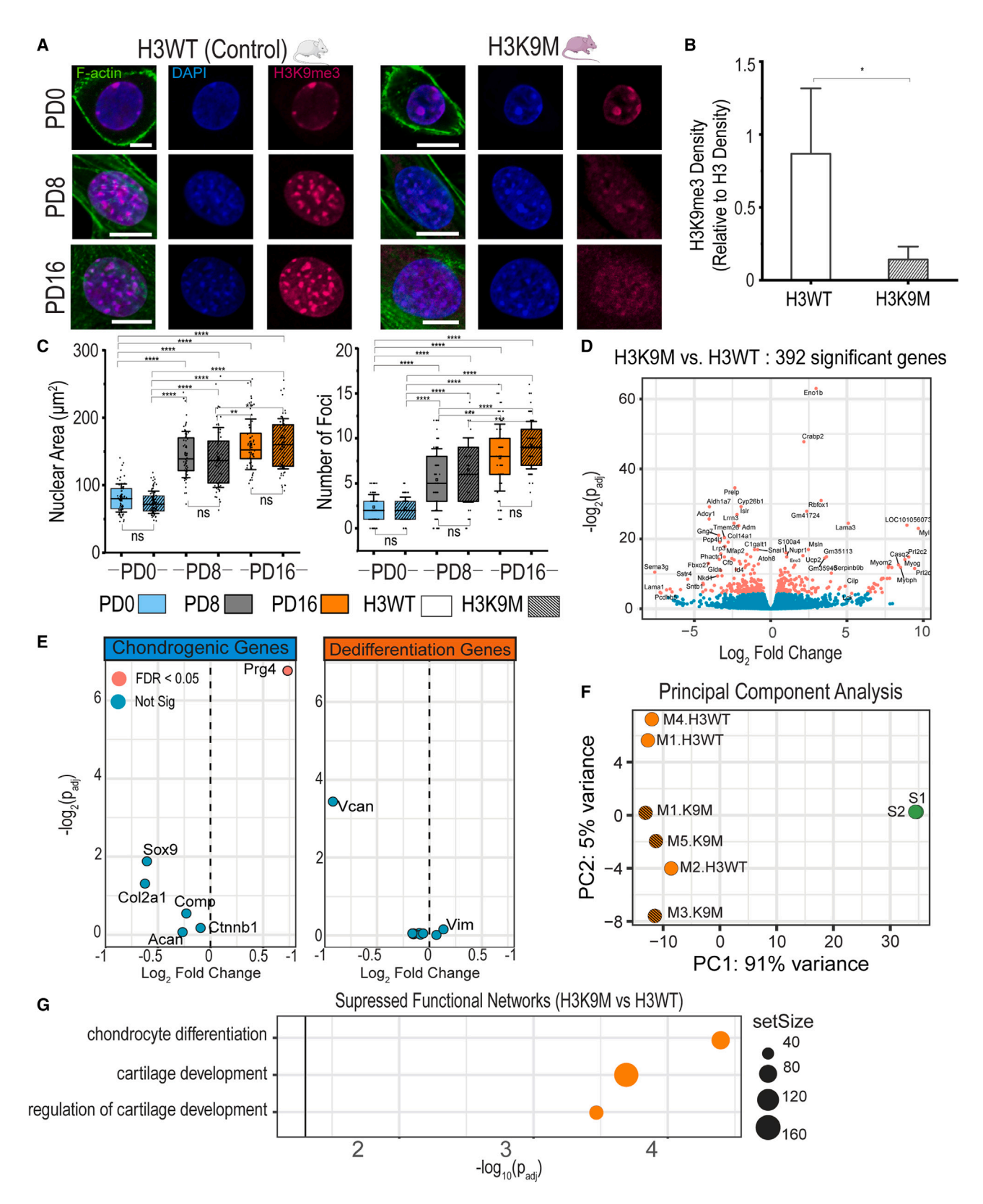


FIGURE 3 Suppression of H3K9me3 did not prevent nuclear architecture remodeling of H3K9 trimethylated chromatin and dedifferentiation of expanded chondrocytes. (A) Chondrocytes were isolated from H3K9M mice or H3WT mice and expanded to PD16. Immunofluorescence imaging showed a decrease in H3K9me3 signal in the H3K9M cells because of the suppressed levels of H3K9me3, but the nuclear architecture changes (H3K9me3 foci) from PD0 to PD16 appeared similar to control cells. (B) Quantified H3K9me3 density relative to total H3 density from Western blots decreased in H3K9M cells compared with

(legend continued on next page)

dedifferentiation (Fig. S2 A). Additionally, we measured mRNA expression of the well-established dedifferentiation genes COL1A1, VCAN, and THY1 (12,48), which increased expression compared with PD0 cells as the chondrocytes became more like fibroblast cells (Fig. 1 E). We hypothesized that a decrease in occupancy levels of repressive marker H3K9me3 would allow for an increase in expression of these genes. We found that the occupancy levels of H3K9me3 on the promoters of chondrocyte dedifferentiation genes (COL1A1, VCAN, THY1) decreased after PD16 compared with the PD0 cells (Fig. 1 F), while H3 density only decreased on the promoter of VCAN (Fig. S2 B). At the same time, gene expression levels of COL1A1 and THY1 increased after PD8, but the occupancy levels of H3K9me3 did not significantly decrease relative to PD0 cells (Fig. 1 F), suggesting that other mechanisms initiated the upregulation of COL1A1 and THY1 of PD8 cells. Altogether, our results showed that a decrease in H3K9me3 occupancy levels is associated with an increased expression of COLIA1, VCAN, and THY1 after PD16 on a 2D stiff substrate. However, the initial change in gene regulation was not driven directly by H3K9me3.

# Recovery of the chondrogenic phenotype depended on the exposure time to 2D culture, establishing a mechanical memory

Next, we encapsulated PD0, PD8, and PD16 chondrocytes in 3D thiol-modified 2% HA-PEGDA hydrogels and analyzed cells after 1, 5, and 10 days in 3D culture to understand if the chromatin architecture of H3K9me3 persisted in 3D culture (Figs. 2, A and B). We assessed the changes in chondrogenic potential, or the ability to regain the hyaline chondrocyte phenotype (redifferentiation) (49), by quantifying gene expression of chondrogenic genes (Fig. 2 C). Compared with PD0-3D controls (chondrocytes encapsulated right after isolation), the chondrogenic gene expression of SOX9 was rescued by encapsulating the cells in hydrogels for 10 days for both the PD8 encapsulated cells (PD8-3D) and PD16 encapsulated cells (PD16-3D) (Fig. 2 C). In contrast, expression levels of COL2A1 and ACAN were not rescued with 3D culture; expression of COL2A1 and ACAN of PD16-3D cells remained significantly lower compared with PD0-3D cells even after 10 days elapsed in 3D culture (Fig. 2 C). The decreased plasticity of the PD16 cells to redifferentiate suggested that the changes in gene expression of select genes (COL2A1, ACAN) in 3D culture depended on the previous exposure time to a stiff 2D substrate.

# Changes in nuclear structure and chromatin architecture of H3K9me3 also depended on the exposure time to 2D culture, demonstrating an intranuclear structural memory

To understand how the dedifferentiated chondrocyte phenotype was retained, we next explored how changes to nuclear morphology and chromatin architecture from 2D culture may be retained in 3D culture. Since we showed that the bulk nuclear properties (e.g., nuclear area and nuclear aspect ratio) changed during dedifferentiation, we investigated if the nuclear area and aspect ratio decreased in subsequent 3D culture as chondrocytes redifferentiated. We determined that after encapsulation of PD8 or PD16 cells, the nuclear aspect ratio did not return to levels of the PD0-3D cells (Fig. S1 B). Notably, we observed a general decrease in nuclear area of all chondrocytes encapsulated in hydrogels compared with the analysis of chondrocytes cultured on TCP (Figs. 1 D and 2 D). However, the nuclear area of PD8-3D and PD16-3D cells significantly decreased after 5 and 10 days in culture, potentially due to the physical constraints of the 3D environment (Fig. 2 D). We confirmed that this decrease in nuclear area was not due to cell death by imaging and analyzing the percentage of viable cells after encapsulation in hydrogels (Fig. S3 A). We also found that the nuclear area of PD16-3D cells decreased over the course of 10 days (Fig. 2 D; p < 0.0001), but PD16-3D cells cultured for 10 days still had larger nuclei compared with PD0-3D cells encapsulated for the same culture time (Fig. 2 D; p < 0.0001). In contrast, the nuclear area of PD8-3D cells decreased after 10 days, approaching levels statistically similar to PD0-3D cells after 1 day in culture (Fig. 2 D; p = 0.2535). The increased adaptability of cells exposed to the stiff TCP for less time (PD8 cells) suggested that the expanded chondrocytes retained a structural nuclear memory of the previous physical environment.

Next, we assessed the intranuclear architecture of H3K9me3 over time in 3D culture. The number of H3K9me3 foci of PD0-3D cells remained low over the course of 10 days (Fig. 2 E). As a control, we cultured ex vivo cartilage plugs to confirm that the hydrogel culture did not change the nuclear architecture of isolated chondrocytes (Fig. S4 A). We found that the chondrocytes cultured ex vivo maintained a

H3WT cells to confirm suppression of H3K9me3 (+SD, N = 4 biological replicates). \*p < 0.05. (C) Nuclear area and number of H3K9me3 foci did not change significantly between H3WT and H3K9M cells of the same passage ( $\pm$ SD, N=4 biological replicates, n>16 nuclei/genotype/replicate). \*p < 0.05, \*\*p < 0.01, \*\*\*\*p < 0.001, \*\*\*\*p < 0.0001, ns: p > 0.05. (D) RNA-seq analysis revealed 392 significantly differentially expressed genes between PD16 H3K9M and H3WT cells. (E) However, most chondrogenic and dedifferentiation genes were not significantly expressed when comparing PD16 H3K9M and H3WT cells. (F) Compared with previously published data of native chondrocytes (samples S1 and S2), principal-component analysis revealed that 91% of the variance of the changes in gene expression in the system can be accounted for by the difference between the expanded (M1-M5 samples) and the native chondrocytes (S1, S2), indicating that both H3K9M and H3WT cells dedifferentiated and differ between them in a much smaller proportion. (G) Although the lack of H3K9me3 did not prevent dedifferentiation, H3K9me3 did play a protective role in maintaining the chondrocyte phenotype since chondrogenic pathways were suppressed significantly for H3K9M cells. To see this figure in color, go online.

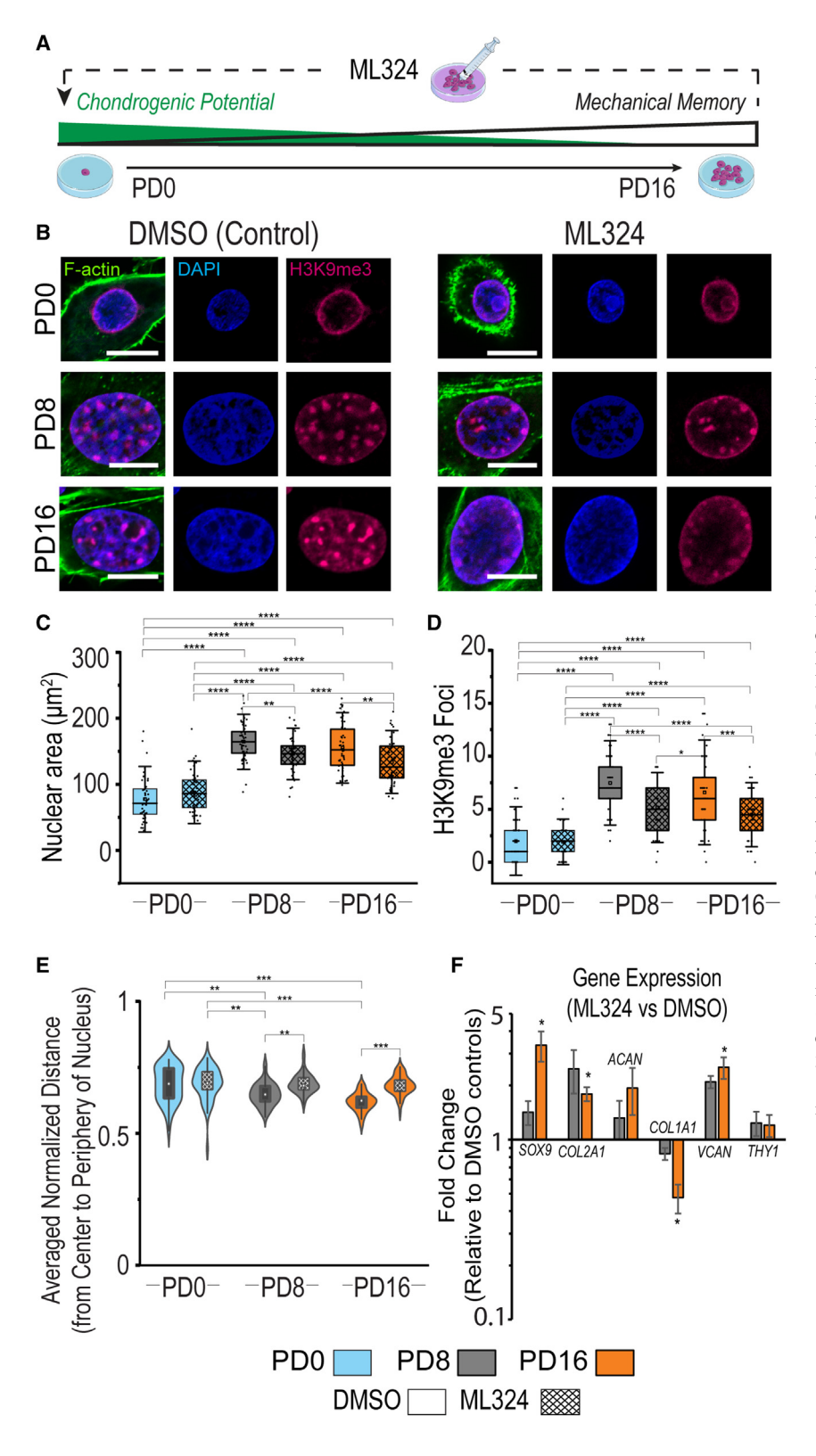


FIGURE 4 Treatment with a KDM4 demethylase inhibitor, ML324, partially maintained chondrogenic nuclear architecture and gene expression. (A) During the expansion process, chondrocytes were treated with a demethylase inhibitor to increase levels of H3K9me3 and enhance the chondrogenic potential of expanded chondrocytes. (B) Chondrocytes were treated with a KDM4 demethylase inhibitor, ML324 (10 µM), or the vehicle control (DMSO) and imaged to assess nuclear architecture of H3K9me3. (C) ML324 treatment decreased the nuclear area of PD8 and PD16 cells compared with PD8 and PD16 DMSO controls ( $\pm$ SD, N = 3 biological replicates, n > 25 nuclei/treatment/replicate). (D) ML324 treatment also decreased the number of H3K9me3 foci compared with DMSO controls. ( $\pm$ SD, N = 3 biological replicates, n > 25 nuclei/ treatment/replicate). (E) The average foci location within the nucleus shifts from the periphery (1) to the center (0) of the cell to PD16; however, the ML324 treatment causes a shift in the distribution of foci location toward the periphery of the cell (box:  $25^{th}$  to  $75^{th}$  percentile,  $\pm$  SD, N = 3 biological replicates, n > 25 nuclei/treatment/replicate). (F) With the treatment of ML324, the expression of the chondrogenic genes SOX9 and COL2A1 is significantly upregulated and the dedifferentiation gene COL1A1 is significantly downregulated by PD16 compared with DMSO controls (mean  $\pm$  SE, N =3 biological replicates). \*p < 0.05, \*\*p < 0.01, \*\*\*p < 0.001, \*\*\*\*p < 0.0001. To see this figure in color, go online.

similar nuclear architecture to PD0-3D cells with low nuclear area, low number of H3K9me3 foci, and low aspect ratios (Fig. S4 B). The encapsulated PD8 and PD16 cells both had a high number of H3K9me3 foci after 24 h. However, throughout the 10 days in culture, the amount of H3K9me3 foci of the PD8-3D cells decreased to levels statistically similar to PD0-3D cells encapsulated for 1 day (Fig. 2 E; p = 0.1681). At the same time, the mean number of foci observed in the PD16-3D nuclei after 10 days remained higher than the mean number of H3K9me3 foci in the PD0-3D cells encapsulated for 1 day (p < 0.0001). We concluded that the organization of H3K9me3 depended on exposure time to the previous 2D stiff substrate, and thus the encapsulated chondrocytes retained an intranuclear structural memory. Additionally, the recovery of chondrogenic genes correlated with the hyaline chondrocyte chromatin architecture (characterized by low numbers of H3K9me3 foci).

# Dedifferentiation genes did not retain dosedependent memory from the previous environment

Given that the chromatin architecture of H3K9me3 correlated with changes in the chondrocyte phenotype, we hypothesized that occupancy levels of H3K9me3 on a single gene level would regulate the persistence of the dedifferentiated phenotype in 3D culture. We specifically focused on occupation of H3K9me3 on COL1A1, THY1, and VCAN in the 3D culture since the occupation of H3K9me3 decreased during dedifferentiation. When assessing the expression of dedifferentiation genes of encapsulated chondrocytes, we found that the expression levels did not show evidence of a dose-dependent memory from the previous environment. Unlike the expression of the chondrogenic genes after encapsulation (Fig. 2 C), the exposure time to 2D culture prior to encapsulation did not influence the magnitude of the decrease in dedifferentiation gene expression after 10 days in the hydrogel culture (Fig. 2 F). After 10 days, the expression of dedifferentiation genes of both the PD8-3D and the PD16-3D cells decreased to similar levels. However, the average change in expression of all dedifferentiation genes from 1 to 5 days in culture was greater for PD8 cells, suggesting that a memory from the previous culture may have influenced the initial redifferentiation rate. To further understand gene regulation of these dedifferentiation genes in the hydrogels, we performed ChIP on the 1 and 10 day samples and assessed the occupancy levels of H3K9me3 and total H3 on the promoters of the dedifferentiation genes (Figs. 2 G and S2 C). Overall, we found that the occupancy levels of H3K9me3 on the promoter of VCAN and THY1 was lower for PD8-3D and PD16-3D cells compared with PD0-3D cells. Although gene expression of the dedifferentiation genes for PD8-3D and PD16-3D cells decreased over time, we did not find that the occupancy levels of H3K9me3 increased. Instead, we demonstrated that the levels of H3K9me3 on the promoters of COL1A1, VCAN, and THY1 remained at statistically similar levels after 10 days for both PD8-3D and PD16-3D cells. However, the density of total H3 protein on promoters of COL1A1, VCAN, and THY1 of PD8-3D and PD16-3D cells increased to statistically similar levels to PD0-3D cells after 10 days (Fig. S2 C), suggesting that other regulatory mechanisms were important for suppressing these dedifferentiation genes following encapsulation. We did conclude that the occupancy level of H3K9me3 on the promoters of VCAN and THY1 depended on whether the chondrocytes were exposed to a 2D stiff environment previously since PD8-3D and PD16-3D cells had lower levels of H3K9me3 occupancy compared with PD0-3D cells (Fig. 2 G). This observation suggested that epigenetic changes that occurred during dedifferentiation were retained in 3D culture. However, our results indicate that as a whole, occupancy levels of H3K9me3 did not retain a gene level memory of the dedifferentiated state when observing the occupancy of H3K9me3 on COL1A1, VCAN, and THY1.

# Suppressing levels of H3K9 methylation did not prevent chromatin architecture remodeling or dedifferentiation

Because our findings indicated a correlation between the chromatin architecture of H3K9me3 and the chondrocyte phenotype, we explored how decreasing H3K9 methylation could alter chromatin architecture and potentially alter the dedifferentiation process. We cultured chondrocytes from a mouse model with an inducible histone H3K9M, which acts as a global dominant negative inhibitor of H3K9 trimethylation. For controls, we used mice with an inducible expression of H3WT (33). Unexpectedly, the overall chromatin architecture of H3K9M PD16 cells was not disrupted and remained similar to the PD16 H3WT cells (Figs. 3, A) and C, and S1 C). Although the fluorescent intensity of H3K9me3 (Figs. 3 A and S5 B) and the protein content shown by Western blots (Figs. 3 B and S6 A) decreased, the number of H3K9me3 foci, nuclear area, and aspect ratio of H3K9M chondrocytes still increased with exposure time to a 2D stiff mechanical environment (Figs. 3 C and S1 C). Subsequently, we wanted to understand if suppression of H3K9 methylation led to changes in gene expression. With gene expression profiling by RNA-seq, we found significant changes in expression of 392 genes (Fig. 3 D); however, expression of the majority of selected chondrogenic or dedifferentiation genes (Table S1) of H3K9M chondrocytes did not change significantly compared with H3WT control chondrocytes (Fig. 3 E). To understand if there was a difference between the dedifferentiation process of the H3K9M and H3WT chondrocytes, we compared the gene expression profiles to previously published gene expression data collected from murine articular native chondrocytes (41). We found that compared with the native articular chondrocytes, both H3K9M and H3WT cells dedifferentiated (Figs. 3 F and S7). Principal-component analysis revealed that H3K9M and H3WT cells shared similar expression profiles but clustered separately from native chondrocytes, suggesting a similar adaptation to the 2D stiff culture (Fig. 3 F). Expression of chondrogenic genes (Sox9, Col2a1, Acan) for both H3K9M cells and H3WT cells decreased compared with native chondrocytes (Fig. S7 A; Tables S2 and S3). Dedifferentiation genes (Col1a1, Col1a2, Thy1, Vim, Col3a1) all increased compared with native controls (Fig. S7 B; Tables S2 and S3). Vcan expression of H3K9M and H3WT cells did not increase significantly compared with native controls, which is likely due to the development timing of the native chondrocyte cells since Vcan is known to be more actively expressed in developing tissue compared with adult tissue (50). Therefore, the suppression of H3K9me3 did not prevent the chromatin architecture remodeling nor dedifferentiation of chondrocytes when exposed to stiff 2D substates, further supporting our previous findings that changes in chromatin architecture correlated with changes in the chondrocyte phenotype.

Although both H3K9M and H3WT cells dedifferentiated compared with native controls, gene expression differences suggest that H3K9me3 was involved in regulating the chondrocyte cell fate through influencing other pathways that are not directly related to dedifferentiation. Decreased H3K9me3 in mutant histone samples altered the expression of genes that were related to cell fate commitment (Fig. S6 B), which was expected since H3K9me3 is a critical epigenetic modification during the differentiation process (51). While individual dedifferentiation genes did not change significantly between H3WT and H3K9M samples, functional annotation revealed that gene expression signatures characteristic of chondrocytes were deenriched in H3K9M samples (Fig. 3 G). Assessment of the significantly changing genes in these pathways revealed several downregulated genes (e.g. Pth1r, Nkx3-4, Grem-1, Snai2, Chadl) that lead to an osteogenic lineage when suppressed (Fig. S6 C) (52-54). Overall, our results indicated that the presence of H3K9me3 does protect a subset of specific chondrogenic functional pathways, but the suppression of H3K9me3 does not significantly influence the dedifferentiation process.

# Demethylase inhibition partially restored both chondrogenic H3K9me3 chromatin architecture and gene expression following expansion on a stiff 2D substrate

Since suppressing H3K9 methylation was not successful in preventing the remodeling of chromatin architecture and the dedifferentiation process, we hypothesized that inhibiting a demethylase of H3K9me3, KDM4, throughout the expansion process would retain the chondrogenic chromatin architecture and increase the chondrogenic potential of expanded chondrocytes (Fig. 4 A). This hypothesis is also supported by our ChIP experimental findings since the loss of H3K9me3 occupancy levels correlated with the loss of the chondrocyte identity (Fig. 1 F). Additionally, we found that the average normalized intensity of H3K9me3 decreased with expansion time (Fig. S5 A), suggesting that increasing levels of H3K9me3 may protect the

chondrogenic phenotype. When we treated cells with a KDM4 inhibitor, ML324 (55), throughout the expansion process, we confirmed that the ML324 treatment increased levels of H3K9me3 intensity through imaging (Fig. S5 C). During the expansion process, we found that chromatin architecture (H3K9me3 foci, nuclear area) of ML324treated cells changed significantly compared with the vehicle control (DMSO) cells (Figs. 4, B–D), yet the nuclear aspect ratio did not change significantly compared with DMSO controls (Fig. S1 D). With ML324, we found that not only did the number of foci change but also the location of the foci. Most foci in the treated cells appeared to be concentrated around the periphery of the nucleus rather than evenly throughout the nucleus like the DMSO controls (Fig. 4 B). To quantify the shift in location of the foci, we calculated the average normalized distance of all foci from the center of the nucleus (value of 1 means the foci was found toward the nuclear envelope, while a value of 0 means the foci was at the center of the nucleus). We found that the average distance of foci from the periphery to the center was lower for PD8 and PD16 DMSO control cells (Fig. 4 E). However, with the ML324 treatment, the average foci location from the center was higher and statistically similar to the PD0 cells (Fig. 4 E). Additionally, ML324 treatment led to a significant increase in expression of SOX9 and COL2A1 and a decrease in expression of COL1A1 but did not decrease the expression of dedifferentiation gene VCAN (Fig. 4 F). When comparing the cell morphology of the ML324 expanded (PD16) cells compared with the expanded (PD16) DMSO controls, we found that the ML324-treated cells displayed less stress fibers, and the overall actin intensity decreased (Fig. S8 A). When comparing the gene expression of the PD16 ML324 cells with the PD16-3D 1 day cells, we found that COL1A1 expression was lower and that COL2A1 expression increased with the ML324-treated cells, while the gene expression of other genes was statistically similar (Fig. S8 B). We also compared the gene expression of the PD16 cells treated with ML324 with the gene expression of PD0 cells and found that while the treatment does increase chondrogenic gene expression compared with untreated PD16 cells, the treatment does not maintain the PD0 state (Fig. S8 C). Taken together, our results suggested that increasing levels of H3K9me3, by inhibiting KDM4 enzymes throughout the expansion process, partially protected the chondrogenic phenotype by maintaining the chromatin architecture even when cultured on stiff 2D substrates.

# **DISCUSSION**

Our work demonstrated how cellular adaptations to the mechanical environment can be encoded in altered gene regulation through epigenetic modifications. As previously demonstrated in the literature, we observed that longer exposure times to stiff mechanical environments led to decreased cellular plasticity when transferred to new mechanical environments. In our experiments, the plasticity, or ability for cells to change phenotypes, was reflected by alterations in the chromatin architecture of the epigenetic modification H3K9me3. In response to a 2D stiff mechanical environment, the chromatin architecture of chondrocyte cells remodeled. When the chondrocytes were transferred to 3D hydrogels, the nuclear architecture persisted in a dosedependent manner according to exposure time to a 2D stiff environment, demonstrating a structural nuclear memory of H3K9 trimethylated chromatin. Notably, the chromatin architecture of PD16 cells exposed to a 2D stiff substrate persisted for at least 10 days. We also found that the change in gene expression over a specified time in 3D culture was greater for PD8-3D than PD16-3D cells, supporting the idea that PD8-3D cells were more able to adapt quickly. Therefore, transfer to a 3D environment only rescued the chondrogenic potential of cells that had been exposed to a stiff 2D substrate for less time (as in the case of PD8 cells).

To understand the role of H3K9me3 in regulating the chondrocyte phenotype, we suppressed levels of H3K9me3. Surprisingly, we found that lower levels of H3K9me3 did not influence the dedifferentiation processes significantly. However, we noticed that the heterochromatin remodeling characteristic of the dedifferentiated phenotype still occurred. When inhibiting the demethylase of H3K9me3 and effectively increasing levels of H3K9me3, the typical chromatin remodeling of the dedifferentiation process was partially prevented, which was also associated with increased expression of chondrogenic genes. Therefore, we speculate that the chromatin architecture of H3K9me3, not necessarily the levels of H3K9me3, was associated with maintaining the chondrocyte phenotype.

The decreased plasticity due to an exposure to a stiff 2D mechanical environment suggested there was a limit to 2D expansion time before cells no longer adapt to new environments. Specifically, for cartilage defect repair, these data suggested that after expanding chondrocytes for PD16, the chondrogenic potential, measured by changes in gene expression of chondrogenic genes, decreased. However, the dose-dependent mechanism that causes the change in chromatin architecture is still unknown. Other studies have demonstrated the role of nuclear localization of transcriptional regulators (YAP/TAZ), which retained a memory induced by exposure to stiff cultures and promoted an osteogenic lineage (6). Similarly, levels of microRNA-21 expression have been shown to preserve a fibrotic cell fate in rat mesenchymal stem cells, and the knockdown of microRNA-21 erased the accumulated memory from priming on stiff substrates (4). Perhaps, over time, the interaction and balance between less stable and more stable gene regulatory mechanisms determined the threshold between reversible and irreversible memory, and thus determined a loss in plasticity, similar to a ball becoming more stable while rolling down into a valley of Waddington's landscape (Fig. 5) (56). For example, we found that as chondrocytes dedifferentiated, the occupancy levels of H3K9me3 decreased by PD16 on dedifferentiation genes COL1A1, VCAN, and THY1. However, the levels of H3K9me3 were not lost at PD8, while the expression of these genes already increased. It is possible that the loss of H3K9me3 was a more stable epigenetic change, suggesting the PD16 cells were less plastic, represented as a ball in a deeper valley in Fig. 5. Future work should explore how the interaction between H3K9me3 and other epigenetic mechanisms, such as DNA methylation, histone methylation, or histone acetylation, could contribute to the overall memory of gene expression. For example, although the occupancy levels of H3K9me3 of the PD8 cells remained elevated on the promoters of dedifferentiation genes, other epigenetic mechanisms (e.g., histone acetylation) or transcriptional regulators could be activating the expression of these genes, and these mechanisms of gene regulation could be less stable or more transient. Alternatively, regulation of the chromatin architecture could stem from the connection to the cytoskeleton through the LINC complex. Our lab has previously shown that dedifferentiation of chondrocytes was associated with a decrease in expression of nuclear envelope and LINC complex proteins, such as lamin A/C and nesprins 1 and 2 (18). We hypothesize that dose-dependent changes in nuclear envelope proteins could alter the chromatin architecture, as shown previously (57). Changes in nuclear envelope proteins may also alter the mechanical properties of the nucleus, such as altering the viscoelastic response (58). In turn, the nucleus could be more susceptible to plastic deformation rather than elastic deformation, similar to how the previously described "motor-clutch" mechanism depends on the balance between elastic and plastic deformation in response to increased actomyosin tension due to a stiff environment (59). Future work could disrupt the protein expression of nuclear envelope proteins or the LINC complex to explore how the nuclear integrity influences the accumulation of memory and chromatin remodeling. Overall, understanding how cellular plasticity is controlled by the mechanical environment through changes in epigenetic factors could provide information to reverse the effects of cell expansion or optimize cellular programming for tissue regeneration procedures.

One notable change in the nucleus of the dedifferentiated chondrocyte was the increased number of H3K9me3 foci. From a biophysics perspective, the formation of these heterochromatin foci could be driven by liquid-liquid phase separation, in which interactions between multivalent macromolecules can cause the formation of separated compartments (60). Functionally, these foci regions may have represented chromocenters, composed of clusters of pericentromeres and characterized by methylated DNA and the occupation of H3K9me2/me3 bound to HP1 (61), but we did not confirm this experimentally. Since centromeres are responsible for correct chromosome segregation during

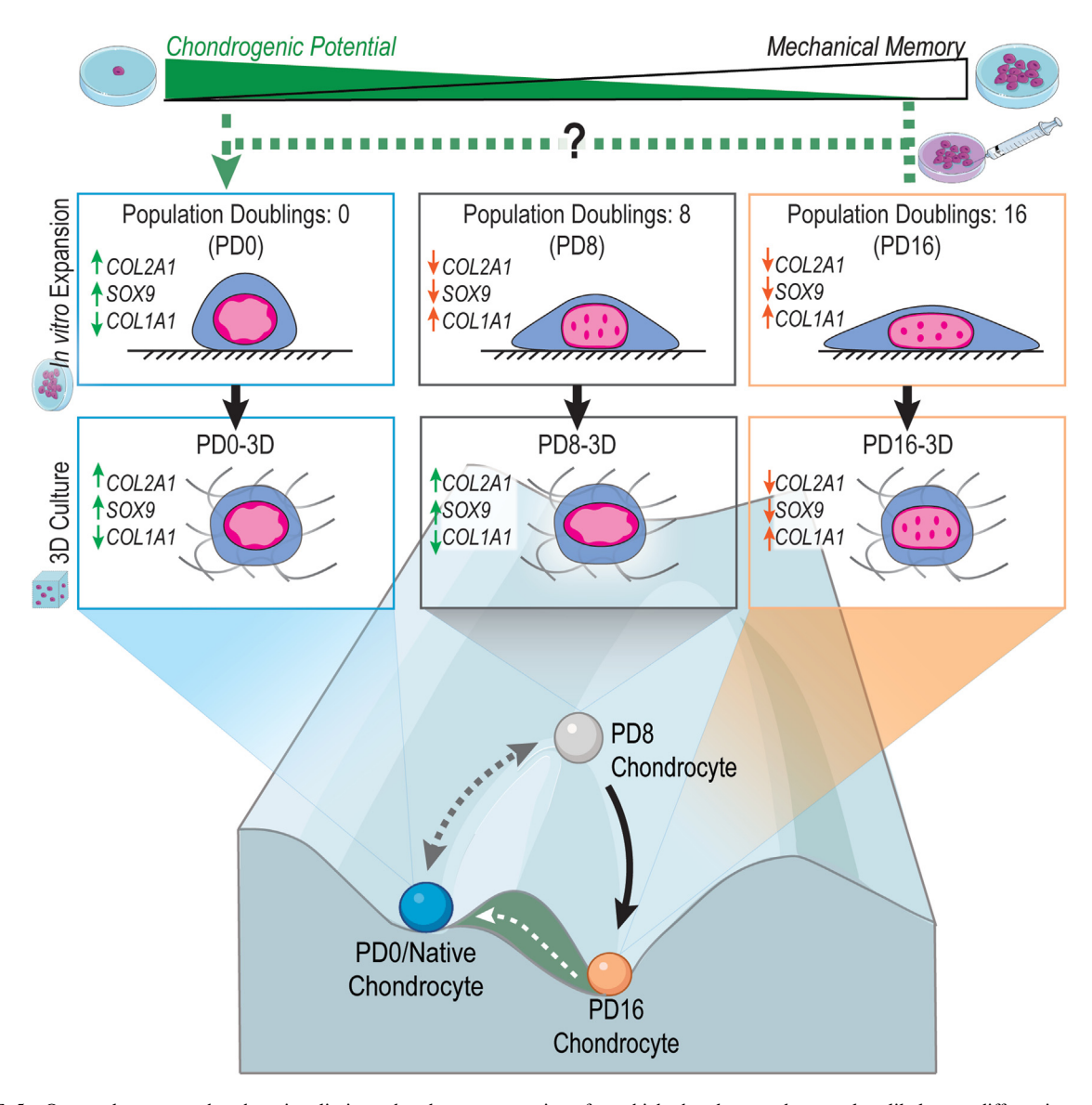


FIGURE 5 Our work suggests that there is a limit to chondrocyte expansion after which chondrocytes become less likely to redifferentiate, which we represent as the PD16 ball rolling into a separate valley on Waddington's landscape. Before reaching this less plastic state, in the PD8 state, chondrocytes still have a greater potential to redifferentiate to the PD0 or native chondrocyte state when encapsulated in a 3D environment. Our results suggest that treatments to inhibit epigenetic modifiers can reduce epigenetic barriers (shown in green), so PD16 cells are more likely to redifferentiate to the PD0 chondrocyte state. To see this figure in color, go online.

cell division (61), it would make sense that these chromocenters may be more evenly distributed and accessible for chromatin organization as the number of PDs increases because chondrocytes are known to divide much more quickly on 2D TCP environments when compared with 3D environments or in vivo (49). Perhaps the increased cell division required reorganization of chromatin architecture to distribute chromocenters throughout the cell for efficient segregation of chromosomes. Future work is needed to explore how the nuclear architecture of PD0 chondrocytes changes in response to cell division. Since our data indicate that the most substantial change in chromatin remodeling occurred between the PD0 and the PD8 states, exploring temporal changes in the first cell divisions and experimentally testing if the H3K9me3 foci coincide with chromocenters will likely provide insight into the functional importance of the H3K9me3 foci.

In addition to the number of foci, we found that there was a shift in localization of H3K9me3 from the periphery of the nucleus to being distributed throughout the nucleus during dedifferentiation. Specifically, we highlight how the ML324 treatment partially restores the increased localization of H3K9me3 toward the nuclear envelope. As genes not necessary for cell identity are generally repressed in the lamina-associated domains (LADs), and as genes that are actively transcribed are more likely found toward the center (62,63), this change in chromatin architecture may reflect a shift in cell phenotype and may represent the activation of genes not necessary for the hyaline chondrocyte function. For example, we hypothesize that the location of chondrocyte dedifferentiation genes (e.g., COL1A1, VCAN, THY1) would be found more toward the center of the nucleus as they become activated during the dedifferentiation process, while chondrogenic genes (e.g., COL2A1, ACAN, SOX9) may be found closer to the periphery as they become suppressed. Future work using DNA fluorescence in situ hybridization could explore the localization of chondrogenic and dedifferentiation genes to understand the role of chromatin organization.

The chromatin remodeling in response to the 2D stiff environment could be partially due to the changes in cytoskeleton structure during dedifferentiation. Mechanical strain can cause cytoskeleton remodeling, increased accumulation of nuclear envelope proteins such as emerin, and global chromatin rearrangements, including decreased localization of H3K9me2/me3 in the LADs (57). Because the LADs are connected to the cytoskeleton through the LINC complex, the reorganization of chromatin in response to changes in the cytoskeleton is plausible. Additionally, previous work disrupting the cytoskeleton of chondrocytes has been beneficial to attenuate the dedifferentiated state (46,64). We postulate that the shift in chromatin architecture could partially be due to the drastic changes in the cytoskeleton that are known to disrupt the organization of H3K9me3. When the chondrocytes are encapsulated, the cellular morphology changes, and the actin cytoskeleton remodels again. Consistent with previous literature, the change in cell morphology is related to a more chondrogenic phenotype (19). Although we observed a dose-dependent memory, the 3D culture eventually rescued the expression of SOX9, a master regulator of chondrogenesis, over time in 3D culture. Perhaps this change in gene expression is due to the change in nuclear tension from the 3D environment, as expression of SOX9 has been shown to be influenced by the mechanical environment (28). Although the 3D environment rescues the expression of SOX9, our experiments show that epigenetic changes persist even with the change in cytoskeleton structure, suggesting that other interventions could enhance the effects of 3D encapsulation.

For this reason, we explored the effect of an epigenetic treatment on chondrocytes during the dedifferentiation process. Epigenetic treatments are increasingly being approved by the FDA, supporting the feasibility of using epigenetic treatments clinically (65-68). Additionally, many epigenetic treatments have been shown to be useful to direct the chondrocyte phenotype (13,69). We found that the demethylase inhibitor ML324 altered the chromatin architecture to appear more similar to that of native hyaline chondrocytes, despite the persistent biophysical cues from the in vitro expansion process. However, the chondrocyte phenotype was not completely restored to the original native state. Future work should be done to assess the advantage of ML324 and other epigenetic treatments in combination with a return to 3D culture to increase the chondrogenic potential of cultured chondrocytes.

Although the results from this study provide valuable insight into how epigenetic remodeling is associated with changes in chondrocyte cell fate, several limitations of this study should be noted. While the HA-PEGDA hydrogels presented an ideal tunable system to ensure a chondrogenic response (36), this environment does not mimic the exact collagen I/III matrix used in the MACI procedure or the native cartilage in the knee joint. With an instantaneous modulus of around 70 kPa and an equilibrium modulus around 25 kPa (36), 2% HA-PEGDA gels are much less stiff compared with native cartilage (70). However, the stiffness more closely matches that of the collagen I/III matrix used in the MACI procedure (71). Additionally, the porosity of a 2% HA-PEGDA gel (5–10  $\mu$ m (72)) may also influence the redifferentiation process. Future studies could explore how varying the mechanical and physical properties of the HA-PEGDA gels could influence chondrocyte cell fate. An additional limitation of our study is that the KDM4 inhibitor affects both the demethylation of H3K9me3 and H3K36me3 (45). Therefore, changes in chromatin architecture could also be due to remodeling of the activation marker H3K36me3, not only H3K9me3. However, since we were most interested in heterochromatin changes, we chose to use ML324 instead of a broad demethylase inhibitor (e.g., JIB-04) since this demethylase inhibitor would also influence other heterochromatin markers, such as H3K27me3 (73).

#### CONCLUSIONS

Taken as a whole, our results reveal the influence of the mechanical environment on cellular plasticity and the role of chromatin remodeling during dedifferentiation and in response to physical cues. An enigma of chromatin regulation is how epigenetic changes provide both stability and cellular plasticity to internal and external signals. Our work addresses this question, showing that exposure time to a stimulus determines the stability and plasticity of cellular responses. Overall, a deeper understanding of how the physical environment influences chromatin remodeling and gene regulation could both improve strategies for tissue regeneration and provide critical information about diseases and development.

#### SUPPORTING MATERIAL

Supporting material can be found online at https://doi.org/10.1016/j.bpj. 2023.03.004.

#### **AUTHOR CONTRIBUTIONS**

Conceptualization, A.K.S. and C.P.N.; methodology, A.K.S., E.C., S.E.S., B.S., J.F.K., J.L.S., J.B., and C.P.N.; formal analysis, A.K.S. and E.C.; investigation, A.K.S., E.C., S.E.S., A.R.S., J.E.B., J.L.S., and K.J.F.; statistical analysis: C.L.V.D.E., A.K.S., and N.C.E.; writing – original draft, A.K.S.; writing – review & editing, all authors; funding acquisition, C.P.N.

#### **ACKNOWLEDGMENTS**

We are grateful for the support from Dr. Thomas Cech and would like to thank the Cech lab for sharing their protocol and resources to learn the chromatin immunoprecipitation process. Additionally, we would like to thank the Genomics Shared Resource Facility at the UC Anschutz Medical Campus for library preparation and RNA-seq of our samples. This work was supported in part by grants to C.P.N. (NIH R01 AR063712, NSF CMMI CAREER 1349735, and NSF CMMI 2212121). J.B. is grateful for support from the NIH R35 GM142884 and Boettcher Foundation's Webb-Waring Biomedical Research Awards program. S.E.S. was funded through NIH T32 GM-065103. J.L.S. was supported by a postdoctoral fellowship 127621-PF-16-099-01-DMC from the American Cancer Society.

#### **DECLARATION OF INTERESTS**

The authors declare no competing interests.

#### **REFERENCES**

- Baker, B. M., and C. S. Chen. 2012. Deconstructing the third dimension how 3D culture microenvironments alter cellular cues. *J. Cell Sci.* 125:3015–3024.
- Engler, A. J., S. Sen, ..., D. E. Discher. 2006. Matrix elasticity directs stem cell lineage specification. *Cell*. 126:677–689.
- Heo, S. J., S. D. Thorpe, ..., R. L. Mauck. 2015. Biophysical regulation of chromatin architecture instills a mechanical memory in mesenchymal stem cells. Sci. Rep. 5:16895.
- Li, C. X., N. P. Talele, ..., B. Hinz. 2017. MicroRNA-21 preserves the fibrotic mechanical memory of mesenchymal stem cells. *Nat. Mater.* 16:379–389.
- Killaars, A. R., J. C. Grim, ..., K. S. Anseth. 2019. Extended exposure to stiff microenvironments leads to persistent chromatin remodeling in human mesenchymal stem cells. Adv. Sci. 6:1801483.
- Yang, C., M. W. Tibbitt, ..., K. S. Anseth. 2014. Mechanical memory and dosing influence stem cell fate. *Nat. Mater.* 13:645–652.
- Balestrini, J. L., S. Chaudhry, ..., B. Hinz. 2012. The mechanical memory of lung myofibroblasts. *Integr. Biol.* 4:410–421.
- 8. Dai, E. N., S. J. Heo, and R. L. Mauck. 2020. Looping in" mechanics: mechanobiologic regulation of the nucleus and the epigenome. *Adv. Healthc. Mater.* 9:2000030.
- 9. Walker, C. J., C. Crocini, ..., K. S. Anseth. 2021. Nuclear mechanosensing drives chromatin remodelling in persistently activated fibroblasts. *Nat. Biomed. Eng.* 5:1485–1499.
- Nasrollahi, S., C. Walter, ..., A. Pathak. 2017. Past matrix stiffness primes epithelial cells and regulates their future collective migration through a mechanical memory. *Biomaterials*. 146:146–155.
- Kim, H. R., and C.-M. Hai. 2005. Mechanisms of mechanical strain memory in airway smooth muscle. *Can. J. Physiol. Pharmacol.* 83:811–815.
- Ma, B., J. C. H. Leijten, ..., M. Karperien. 2013. Gene expression profiling of dedifferentiated human articular chondrocytes in monolayer culture. *Osteoarthritis Cartilage*. 21:599–603.
- Duan, L., Y. Liang, ..., D. Wang. 2015. Epigenetic regulation in chondrocyte phenotype maintenance for cell-based cartilage repair. Am. J. Transl. Res. 7:2127–2140.
- Committee for Medicinal Products for Human Use (CHMP). 2013.
   Assessment Report MACI Common Name: Matrix Applied Characterised Autologous Cultured Chondrocytes. European Medicines Agency.

- Lin, Z., C. Willers, ..., M.-H. Zheng. 2006. The chondrocyte: biology and clinical application. *Tissue Eng.* 12:1971–1984.
- Barlic, A., M. Drobnic, ..., N. Kregar-Velikonja. 2008. Quantitative analysis of gene expression in human articular chondrocytes assigned for autologous implantation. J. Orthop. Res. 26:847–853.
- Schnabel, M., S. Marlovits, ..., J. Schlegel. 2002. Dedifferentiationassociated changes in morphology and gene expression in primary human articular chondrocytes in cell culture. *Osteoarthritis Cartilage*. 10:62–70.
- Ghosh, S., A. K. Scott, ..., C. P. Neu. 2022. Dedifferentiation alters chondrocyte nuclear mechanics during in vitro culture and expansion. *Biophys. J.* 121:131–141.
- Benya, P. D., and J. D. Shaffer. 1982. Dedifferentiated chondrocytes reexpress the differentiated collagen phenotype when cultured in agarose gels. *Cell.* 30:215–224.
- Tallheden, T., C. Karlsson, ..., A. Lindahl. 2004. Gene expression during redifferentiation of human articular chondrocytes. *Osteoarthr. Cartil*. 12:525–535.
- Schulze-Tanzil, G., A. Mobasheri, ..., M. Shakibaei. 2004. Loss of chondrogenic potential in dedifferentiated chondrocytes correlates with deficient Shc–Erk interaction and apoptosis. *Osteoarthr. Cartil*. 12:448–458.
- Fan, X., L. Zhu, ..., Y. Du. 2017. Stiffness-controlled thermoresponsive hydrogels for cell harvesting with sustained mechanical memory. Adv. Healthc. Mater. 6:1601152.
- Thienpont, B., J. M. Aronsen, ..., H. L. Roderick. 2017. The H3K9 dimethyltransferases EHMT1/2 protect against pathological cardiac hypertrophy. J. Clin. Invest. 127:335–348.
- Pombo, A., and N. Dillon. 2015. Three-dimensional genome architecture: players and mechanisms. *Nat. Rev. Mol. Cell Biol.* 16:245–257.
- Turner, B. M. 2002. Cellular memory and the histone code. Cell. 111:285–291.
- Hathaway, N. A., O. Bell, ..., G. R. Crabtree. 2012. Dynamics and memory of heterochromatin in living cells. Cell. 149:1447–1460.
- Brumbaugh, J., B. Di Stefano, and K. Hochedlinger. 2019. Reprogramming: identifying the mechanisms that safeguard cell identity. *Development*. 146:dev182170.
- Maki, K., M. M. Nava, ..., S. A. Wickström. 2021. Hydrostatic pressure prevents chondrocyte differentiation through heterochromatin remodeling. *J. Cell Sci.* 134:jcs247643.
- Seelbinder, B., S. Ghosh, ..., C. P. Neu. 2021. Nuclear deformation guides chromatin reorganization in cardiac development and disease. *Nat. Biomed. Eng.* 5:1500–1516.
- Novak, T., K. Fites Gilliland, ..., C. P. Neu. 2016. In vivo cellular infiltration and remodeling in a decellularized ovine osteochondral allograft. *Tissue Eng. Part A*. 22:1274–1285.
- Neu, C. P., A. Khalafi, ..., A. H. Reddi. 2007. Mechanotransduction of bovine articular cartilage superficial zone protein by transforming growth factor signaling. *Arthritis Rheum*. 56:3706–3714.
- Eng, D., M. Caplan, ..., A. Panitch. 2010. Hyaluronan scaffolds: a balance between backbone functionalization and bioactivity. *Acta Biomater*. 6:2407–2414.
- Brumbaugh, J., I. S. Kim, ..., K. Hochedlinger. 2019. Inducible histone K-to-M mutations are dynamic tools to probe the physiological role of site-specific histone methylation in vitro and in vivo. *Nat. Cell Biol.* 21:1449–1461.
- Jonason, J. H., D. Hoak, and R. J. O'Keefe. 2015. Primary murine growth plate and articular chondrocyte isolation and cell culture. *Methods Mol. Biol.* 1226:11–18.
- Seelbinder, B., A. K. Scott, ..., C. P. Neu. 2020. TENSCell: imaging of stretch-activated cells reveals divergent nuclear behavior and tension. *Biophys. J.* 118:2627–2640.
- Barthold, J. E., B. M. Martin, ..., C. P. Neu. 2021. Recellularization and integration of dense extracellular matrix by percolation of tissue microparticles. Adv. Funct. Mater. 31:2103355.

- Kim, D., J. M. Paggi, ..., S. L. Salzberg. 2019. Graph-based genome alignment and genotyping with HISAT2 and HISAT-genotype. *Nat. Biotechnol.* 37:907–915.
- Liao, Y., G. K. Smyth, and W. Shi. 2014. featureCounts: an efficient general purpose program for assigning sequence reads to genomic features. *Bioinformatics*. 30:923–930.
- Love, M. I., W. Huber, and S. Anders. 2014. Moderated estimation of fold change and dispersion for RNA-seq data with DESeq2. *Genome Biol.* 15:550.
- Yu, G., L. G. Wang, ..., Q. Y. He. 2012. clusterProfiler: an R package for comparing biological themes among gene clusters. *OMICS*. 16:284–287.
- Wuelling, M., C. Neu, ..., A. Vortkamp. 2021. Epigenetic mechanisms mediating cell state transitions in chondrocytes. *J. Bone Miner. Res.* 36:968–985.
- Ramírez, F., F. Dündar, ..., T. Manke. 2014. deepTools: a flexible platform for exploring deep-sequencing data. *Nucleic Acids Res.* 42:W187–W191.
- Cotney, J. L., and J. P. Noonan. 2015. Chromatin immunoprecipitation with fixed animal tissues and preparation for high-throughput sequencing. Cold Spring Harb. Protoc. 2015:199–419.
- Stern, J. L., D. Theodorescu, ..., T. R. Cech. 2015. Mutation of the TERT promoter, switch to active chromatin, and monoallelic TERT expression in multiple cancers. *Genes Dev.* 29:2219–2224.
- Dobrynin, G., T. E. McAllister, ..., E. M. Hammond. 2017. KDM4A regulates HIF-1 levels through H3K9me3. Sci. Rep. 7:11094.
- 46. Rottmar, M., R. Mhanna, ..., K. Maniura-Weber. 2014. Interference with the contractile machinery of the fibroblastic chondrocyte cytoskeleton induces re-expression of the cartilage phenotype through involvement of PI3K, PKC and MAPKs. Exp. Cell Res. 320:175–187.
- Darling, E. M., and K. A. Athanasiou. 2005. Rapid phenotypic changes in passaged articular chondrocyte subpopulations. *J. Orthop. Res.* 23:425–432.
- Diaz-Romero, J., J. P. Gaillard, ..., P. Mainil-Varlet. 2005. Immunophenotypic analysis of human articular chondrocytes: changes in surface markers associated with cell expansion in monolayer culture. *J. Cell. Physiol.* 202:731–742.
- Caron, M. M. J., P. J. Emans, ..., T. J. M. Welting. 2012. Redifferentiation of dedifferentiated human articular chondrocytes: comparison of 2D and 3D cultures. *Osteoarthritis Cartilage*. 20:1170–1178.
- Choocheep, K., S. Hatano, ..., H. Watanabe. 2010. Versican facilitates chondrocyte differentiation and regulates joint morphogenesis. *J. Biol. Chem.* 285:21114–21125.
- Nicetto, D., and K. S. Zaret. 2019. Role of H3K9me3 heterochromatin in cell identity establishment and maintenance. *Curr. Opin. Genet. Dev.* 55:1–10.
- Becher, C., T. Szuwart, ..., C. O. Tibesku. 2010. Decrease in the expression of the type 1 PTH/PTHrP receptor (PTH1R) on chondrocytes in animals with osteoarthritis. J. Orthop. Surg. Res. 5:28.
- Worthley, D. L., M. Churchill, ..., T. C. Wang. 2015. Gremlin 1 identifies a skeletal stem cell with bone, cartilage, and reticular stromal potential. *Cell*. 160:269–284.
- Razmara, E., A. Bitaraf, ..., S. Babashah. 2021. Functions of the SNAI family in chondrocyte-to-osteocyte development. *Ann. N. Y. Acad. Sci.* 1503:5–22.

- Zhang, B., Q. Long, ..., Y. Sun. 2021. KDM4 orchestrates epigenomic remodeling of senescent cells and potentiates the senescence-associated secretory phenotype. *Nat. Aging.* 1:454–472.
- Noble, D. 2015. Conrad Waddington and the origin of epigenetics. J. Exp. Biol. 218:816–818.
- Le, H. Q., S. Ghatak, ..., S. A. Wickström. 2016. Mechanical regulation of transcription controls Polycomb-mediated gene silencing during lineage commitment. *Nat. Cell Biol.* 18:864–875.
- Swift, J., I. L. Ivanovska, ..., D. E. Discher. 2013. Nuclear lamin-A scales with tissue stiffness and enhances matrix-directed differentiation. *Science*. 341:1240104.
- Zhang, C., H. Zhu, ..., M. Lin. 2021. Mechanics-driven nuclear localization of YAP can be reversed by N-cadherin ligation in mesenchymal stem cells. *Nat. Commun.* 12:6229.
- Wang, L., Y. Gao, ..., P. Li. 2019. Histone modifications regulate chromatin compartmentalization by contributing to a phase separation mechanism. *Mol. Cell.* 76:646–659.e6.
- Probst, A. v., E. Dunleavy, and G. Almouzni. 2009. Epigenetic inheritance during the cell cycle. *Nat. Rev. Mol. Cell Biol.* 10:192–206.
- Shah, P. P., W. Lv, ..., R. Jain. 2021. Pathogenic LMNA variants disrupt cardiac lamina-chromatin interactions and de-repress alternative fate genes. *Cell Stem Cell*. 28:938–954.e9.
- Poleshko, A., P. P. Shah, ..., R. Jain. 2017. Genome-nuclear lamina interactions regulate cardiac stem cell lineage restriction. *Cell.* 171:573

  587 e14
- Parreno, J., M. Nabavi Niaki, ..., R. A. Kandel. 2017. Interplay between cytoskeletal polymerization and the chondrogenic phenotype in chondrocytes passaged in monolayer culture. *J. Anat.* 230:234–248.
- Stratton, M. S., and T. A. McKinsey. 2016. Epigenetic regulation of cardiac fibrosis. J. Mol. Cell. Cardiol. 92:206–213.
- 66. Heerboth, S., K. Lapinska, ..., S. Sarkar. 2014. Use of epigenetic drugs in disease: an overview. *Genet. Epigenet*. 6:9–19.
- Lui, J. C., P. Garrison, ..., J. Baron. 2016. EZH1 and EZH2 promote skeletal growth by repressing inhibitors of chondrocyte proliferation and hypertrophy. *Nat. Commun.* 7:13685.
- Yamamoto, H., K. Schoonjans, and J. Auwerx. 2007. Sirtuin functions in health and disease. *Mol. Endocrinol.* 21:1745–1755.
- Duan, L. I., Y. Liang, ..., D. Wang. 2017. DNA methylation profiling in chondrocyte dedifferentiation in vitro. J. Cell. Physiol. 232:1708–1716.
- Moshtagh, P. R., B. Pouran, ..., A. Zadpoor. 2014. The elastic modulus of articular cartilage at nano-scale and micro-scale measured using indentation type atomic force microscopy. *Osteoarthritis Cartilage*. 22:S359–S360.
- Nixon, A. J., E. Rickey, ..., G. L. Matthews. 2015. A chondrocyte infiltrated collagen type I/III membrane (MACI® implant) improves cartilage healing in the equine patellofemoral joint model. *Osteoar-thritis Cartilage*. 23:648–660.
- Silva Garcia, J. M., A. Panitch, and S. Calve. 2019. Functionalization of hyaluronic acid hydrogels with ECM-derived peptides to control myoblast behavior. *Acta Biomater*. 84:169–179.
- 73. Parrish, J. K., T. S. McCann, ..., P. Jedlicka. 2018. The Jumonji-domain histone demethylase inhibitor JIB-04 deregulates oncogenic programs and increases DNA damage in Ewing Sarcoma, resulting in impaired cell proliferation and survival, and reduced tumor growth. *Oncotarget*. 9:33110–33123.